

Structural and magnetic investigation of $\text{Ca}_2\text{MnReO}_6$ doped with Ce

(Investigação estrutural e magnética de $\text{Ca}_2\text{MnReO}_6$ dopado com Ce)

J. B. Depianti¹, M. T. D. Orlando¹, A. S. Cavichini¹, H. P. S. Corrêa², V. A. Rodrigues¹, J. L. Passamai¹, E. L. O Piedade¹, H. Belich¹, E. F. Medeiros¹, F. C. L. de Melo³

¹Universidade Federal do Espírito Santo, Av. Fernando Ferrari 514, Vitória, ES 29075-910

²Universidade Federal de Mato Grosso do Sul, Campo Grande, MS

³Centro Técnico Aeroespacial - IEA, Pça. Marechal-do-ar Eduardo Gomes, 50, S. José dos Campos, SP 12228-904 Brazil
jdepianti@gmail.com

Abstract

We have studied the properties of Ce doping in Ca-site of $\text{Ca}_2\text{MnReO}_6$ double perovskite up to 10%. These compounds have presented a monoclinic cell with $P2_1/n$ space group. A small increase of lattice parameters in doped sample were observed through Rietveld refinement of X-ray diffraction pattern. The spectra at the Mn K-edge and Re L_3 -edge showed a mixed valence for Mn and Re in both samples. We do not observed any variation on Mn K-edge valence in XANES measurements under pressure. However a change was observed for Re L_3 -edge as a function of applied pressure. The Ce-doped sample showed a magnetic geometric frustration and a small decrease of the temperature frustration as compared with $\text{Ca}_2\text{MnReO}_6$ sample. The decrease of temperature frustration can be related to the MnO_6 and ReO_6 octahedral distortion.

Keywords: Ce-doping, double perovskite, XANES, pressure.

Resumo

Neste trabalho estudamos as propriedades da dupla perovskita $\text{Ca}_2\text{MnReO}_6$ dopada com até 10% de Ce no sítio do Ca. Estes compostos apresentaram uma célula monoclinica com grupo espacial $P2_1/n$. Através do refinamento do padrão de difração de raios X pelo método de Rietveld observamos um pequeno aumento nos parâmetros de rede para a amostra dopada. Os espectros de absorção de raios X na borda K do Mn e L_3 do Re mostram que o Mn e Re assumem valência mista em ambas as amostras. Nas medidas de XANES sob pressão não observamos nenhuma variação na valência para a borda K do Mn. No entanto, foi observado um deslocamento da borda L_3 do Re para alta energia em função da pressão aplicada. A amostra dopada com Ce apresentou frustração magnética geométrica. Houve um pequeno decréscimo da temperatura de frustração da amostra dopada em comparação com a amostra $\text{Ca}_2\text{MnReO}_6$. A diminuição da temperatura frustração pode estar relacionada com a distorção octaédrica do MnO_6 e do ReO_6 .

Palavras-chave: dopagem com cério, dupla perovskita, XANES, pressão.

INTRODUCTION

After the discovery of the $\text{Sr}_2\text{FeMoO}_6$ compound [1], the electromagnetic ceramics open a new field of investigation about magnetoresistance effect under low-magnetic field at room temperature. These oxide compounds, labeled as double perovskites, exhibit a large magnetic and electronic properties due to strong interplay between crystallographic structure, charge and spin ordering [2], which improve the use of this compound in magnetoelectronic devices [3].

The structure of the $\text{A}_2\text{BB}'\text{O}_6$ double perovskite, proposed by Longo and Ward [4] in 1961, is very similar to ABO_3 simple perovskite. However, the double perovskite presents a solid ordered solution of the BO_6 and $\text{B}'\text{O}_6$ octahedral. The ideal structure is based on the adapted tolerance factor t of simple perovskite [5] taking into account the mixed A-site $\text{A}_{2-x}\text{A}'_x\text{BB}'\text{O}_6$ [6], as can be seen in equation (A):

$$t = \frac{\left(1 - \frac{x}{2}\right)\gamma_A + \frac{x}{2}\gamma_{A'} + \gamma_0}{\sqrt{2} \left(\frac{\gamma_B}{2} + \frac{\gamma_{B'}}{2} + \gamma_0\right)} \quad (\text{A})$$

where γ_A , $\gamma_{A'}$, γ_B and $\gamma_{B'}$ are the ionic radii of the respective ions and γ_0 is the ionic radius of oxygen. According to the value of t , the double perovskite may take different structures: a hexagonal structure for $t > 1.05$, a cubic structure with $Fm\bar{3}m$ space group for $1.05 > t > 1.00$, a $I4/m$ tetragonal space group for $1.00 > t > 0.97$ and $P2_1/n$ monoclinic space group or orthorhombic for $0.97 > t$ [7].

As reported by Philipp *et al.* [8] and Popov *et al.* [9], there is a correlation between the A-site cation size and the magnetic moment saturation of the double perovskites. Other properties have been investigated as a function of doping A-site [10-12], in $\text{Sr}_2\text{FeMoO}_6$ the Curie temperature (T_C)

increases with a partial substitution of Sr for rare-earth (Ln) and, in the $\text{Sr}_2\text{CrReO}_6$ T_C decreases with Nd^{+3} doping [13].

In this work we investigate the effects on $\text{Ca}_2\text{MnReO}_6$ crystal structure and magnetism as a function of partial substitution up to 10% of Ce^{4+} on Ca^{2+} site.

EXPERIMENTAL DETAILS

Synthesis procedure

Polycrystalline $\text{Ca}_2\text{MnReO}_6$ and $\text{Ca}_{1.8}\text{Ce}_{0.2}\text{MnReO}_6$ samples were prepared by solid state reaction of CaO , CeO_2 (Sigma Aldrich 99.995%), MnO_2 (Alfa Aesar, Puratronic 99.9%) and ReO_2 (Sigma Aldrich 99.7%) oxides. The CaO was obtained by decomposition of CaCO_3 (Alfa Aesar, Puratronic 99.999%) heated at 980 °C in O_2 atmosphere for 24 h. Before synthesis procedure, the oxides were heated at 400 °C for 24 h to remove any impurities and humidity. The powder were mixed and pressed in pellets, which were wrapped in gold foil (Alfa Aesar, Puratronic 99.999%) and sealed in a evacuated (10^{-2} torr) quartz tube. The sealed sample was placed in a tubular furnace and heated at a rate of 100 °C/h up to 900 °C, where it remained for 24 h, and then cooled at the same rate down to room temperature. Three intermediate steps of grinding were carried out. The second and third heat treatments were at 980 °C for 48 h. Finally, for the fourth treatment, the pellets were placed in a crucible instead of wrapped in gold foil, and were heated up to 1300 °C for 12 h always using the same rate of heating and cooling.

The oxygen stoichiometry was determined by mass variation and the residual oxygen pressure measured in the quartz tube at room temperature after each thermal treatment, and also considering the analytical balance accuracy (0.0001 g) and the pressure measurement setup accuracy (20 mmHg). The final oxygen stoichiometry was 6.0 ± 0.1 for $\text{Ca}_2\text{MnReO}_6$ and 6.0 ± 0.2 for $\text{Ca}_{1.8}\text{Ce}_{0.2}\text{MnReO}_6$.

Sample characterization

The high-resolution X-ray powder diffraction measurement was performed at the XRD1 beamline of the Brazilian Synchrotron Light Laboratory (LNLS), using a wavelength $\lambda = 1.20368$ Å, at ambient pressure. A Ge(111) analyzer crystal was placed in a goniometer attached to the 2θ arm, and a scintillation detector was used. NIST standard reference material Al_2O_3 was measured in the same experimental conditions in order to obtain the instrumental parameters. The GSAS program [14] with the EXPGUI interface [15] was used for the Rietveld analysis and the structure reported by Corrêa *et al.* [16] was used as the input for the refinement.

The morphology of the particles and their chemical composition were determined using a scanning electron microscope (SEM) together with an X-ray energy dispersive spectrometer (EDS). The SEM observations were carried out at magnifications up to 5,000. The electron beam energy

was 20 keV, and probe current of the order of 25 A.

The X-ray absorption spectroscopy (XAS) measurements were carried out on XAFS1 beamline of the Brazilian Synchrotron Light Laboratory with a Si-111 monochromator in transmission mode on powder samples for Mn K-edge and Re L_3 -edge. More details the XAFS1 can be seen in Ref. 17. For precise energy calibration, manganese metallic and ReO_3 were used with standards and run with the samples during the measurements. MnO , MnO_2 , Mn_2O_3 , ReO_2 and ReO_3 thick films were used as standard compounds. XAS under pressure was measured in B_4C anvil pressure cell using ReO_3 as inner pressure gauge only for the doped sample. Details of the B_4C anvil pressure cell and the settings configuration for XAS measurements under pressure are described in Ref. 18. The XANES were normalized to high energy range of spectrum (~ 100 eV beyond the edge) after background subtraction.

Magnetic characterization of the samples was performed in powder form. The AC magnetic susceptibility at ambient pressure was measured with a homemade calibrated and automated device using a driving field $H_{AC} = 6$ A/m and a frequency $\nu = 448$ Hz [19, 20]. The induced voltage in the astatic pair of pick up coils was detected by a lock-in amplifier 5210, dual phase, EG&G. A Lake-Shore temperature controller, model 310, was used to set the temperature detected with a calibrated GaAlAs-sensor (GAL 8957).

RESULTS AND DISCUSSION

Crystal structure

The results of structural refinements are listed in Table I with the full diffraction pattern displayed in Figs. 1a and 1b.

The calculus of tolerance factor t through the equation (A) using the ionic radii reported by Shannon [21] for both samples is < 0.97 . This result suggests a monoclinic ($P2_1/n$) or orthorhombic structure [7]. Then the monoclinic structure with space group $P2_1/n$ was used to analyze the diffraction pattern in both samples. A major consequence of the distortion is that the Mn—O—Re angle is considerably lower than 180°. The relevant bond-lengths and angles are shown in Table II.

No secondary phases or impurities were observed in the diffraction pattern of $\text{Ca}_2\text{MnReO}_6$ and the structural parameters are the same to the ones reported by Corrêa *et al.* [16] and similar to the ones reported by Kato *et al.* [22]. Residual traces of CeO_2 were found in the $\text{Ca}_{1.8}\text{Ce}_{0.2}\text{MnReO}_6$, which was remarked as second set of tick marks in the diffraction pattern (Fig. 1b). The small content of MnO was also detected, but had no influence in the refinement. The weight percentage was 2.7% for CeO_2 by Rietveld refinement.

The occupation refinement of the Ca and Ce in the sample $\text{Ca}_{1.8}\text{Ce}_{0.2}\text{MnReO}_6$ showed that the real composition is $\text{Ca}_{1.921}\text{Ce}_{0.079}\text{MnReO}_6$. Refinements of occupancy at B and B' sites indicate that the disorder of Mn and Re atoms is

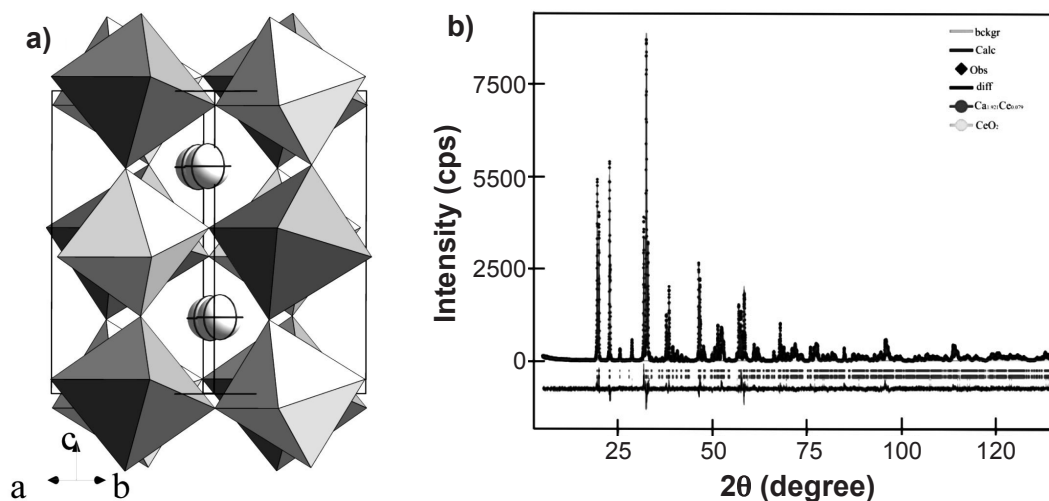


Figure 1: (a) Powder x-ray diffraction refinement of $\text{Ca}_2\text{MnReO}_6$ with $\lambda = 1.20368 \text{ \AA}$. ($R_{\text{wp}} = 0.1093$, $\chi^2 = 2.448$, $R_F^2 = 0.0466$). (b) Powder x-ray diffraction refinement of $\text{Ca}_{1.8}\text{Ce}_{0.2}\text{MnReO}_6$ with $\lambda = 1.20368 \text{ \AA}$. ($R_{\text{wp}} = 0.1280$, $\chi^2 = 2.837$, $R_F^2 = 0.0511$). The second of set tick marks is for a CeO_2 impurity.

[Figura 1: (a) Refinamento do padrão de difração de raios X de pó da amostra $\text{Ca}_2\text{MnReO}_6$ com $\lambda = 1,20368 \text{ \AA}$. ($R_{\text{wp}} = 0,1093$; $\chi^2 = 2,448$; $R_F^2 = 0,0466$). (b) Refinamento do padrão de difração de raios X de pó da amostra $\text{Ca}_{1,8}\text{Ce}_{0,2}\text{MnReO}_6$ com $\lambda = 1,20368 \text{ \AA}$. ($R_{\text{wp}} = 0,1280$; $\chi^2 = 2,837$; $R_F^2 = 0,0511$).]

Table I - Rietveld fit results of the lattice and atomic parameters of samples $\text{Ca}_2\text{MnReO}_6$ and $\text{Ca}_{1.921}\text{Ce}_{0.079}\text{MnReO}_6$. Both samples are monoclinic ($P2_1/n$). The errors represent the standard deviation (statistical only).

[Tabela I - Resultados de refinamentos de Rietveld da rede e dos parâmetros atômicos das amostras $\text{Ca}_2\text{MnReO}_6$ e $\text{Ca}_{1,921}\text{Ce}_{0,079}\text{MnReO}_6$. Ambas amostras tem estrutura monoclinica ($P2_1/n$). Os erros representam o desvio padrão (somente estatístico).]

$\text{Ca}_2\text{MnReO}_6$	a = 5.44445(2) Å	b = 5.63957(3) Å	c = 7.77524(3) Å	$\beta = 90.18(1)^\circ$	Occ.
Atom	x	y	z	Uiso(Å ²)	
Ca	0.4859(5)	0.55514(31)	0.25221(29)	0.0037(1)	1
Mn	1/2	0	1/2	0.0037(1)	1
Re	1/2	0	0	0.0037(1)	1
O1	0.3142(12)	0.2872(12)	0.0481(10)	0.0053(12)	1
O2	0.2124(12)	0.8025(12)	0.0478(10)	0.0053(12)	1
O3	0.5950(11)	-0.0414(12)	0.2443(8)	0.0053(12)	1
$\text{Ca}_{1.921}\text{Ce}_{0.079}\text{MnReO}_6$	a = 5.4578 (3) Å	b = 5.6494 (2) Å	c = 7.7948 (2) Å	$\beta = 90.17(1)^\circ$	Occ.
Atom	x	y	z	Uiso(Å ²)	
Ca	0.4868(6)	0.55037(26)	0.25231(28)	0.0073(5)	0.961
Ce	0.492(5)	0.5700(19)	0.2515(23)	0.0073(5)	0.039
Mn	1/2	0	1/2	0.0039(3)	1
Re	1/2	0	0	0.0060(1)	1
O1	0.3172(11)	0.2824(10)	0.041(1)	0.0083(17)	1
O2	0.2103(11)	0.8370(11)	0.0412(10)	0.0083(17)	1
O3	0.5855(10)	-0.0264(11)	0.2371(7)	0.0083(17)	1

about ~ 3% in both samples. The results of the Rietveld fit for the atomic positions presented in the Table I show that Mn cations occupy the 2d position, Re the 2c position and the Ca/Ce cation and three oxygen anions occupy different 4e

positions. According to Glazer's notation, there is an ab^+ configuration along the pseudo-cubic axes [23]. A positive superscript would denote the neighboring octahedral tilt in the same direction (in-phase) and a negative superscript

Table II - Length and bond angles of $\text{Ca}_2\text{MnReO}_6$ and $\text{Ca}_{1.921}\text{Ce}_{0.079}\text{MnReO}_6$. The errors represent one standard deviation and are statistical only.

[Tabela II - Comprimentos e ângulos de ligação do $\text{Ca}_2\text{MnReO}_6$ e $\text{Ca}_{1.921}\text{Ce}_{0.079}\text{MnReO}_6$. Os erros representam o desvio padrão e são estatísticos somente.]

	MnO_6		ReO_6	
	Ca_2	$\text{Ca}_{1.921}\text{Ce}_{0.079}$	Ca_2	$\text{Ca}_{1.921}\text{Ce}_{0.079}$
Mn-O1(Å)	2.133(6)	2.146(5)	Re-O1	1.940(6)
Mn-O2(Å)	2.109(7)	2.246(6)	Re-O2	1.947(7)
Mn-O3(Å)	2.082(5)	2.108(7)	Re-O3	1.967(5)
			Ca_2	$\text{Ca}_{1.921}\text{Ce}_{0.079}$
Mn-O1-Re(°)			148.4(3)	151.087(4)
Mn-O2-Re(°)			150.2(4)	146.107(3)
Mn-O3-Re(°)			147.5(3)	151.707(3)

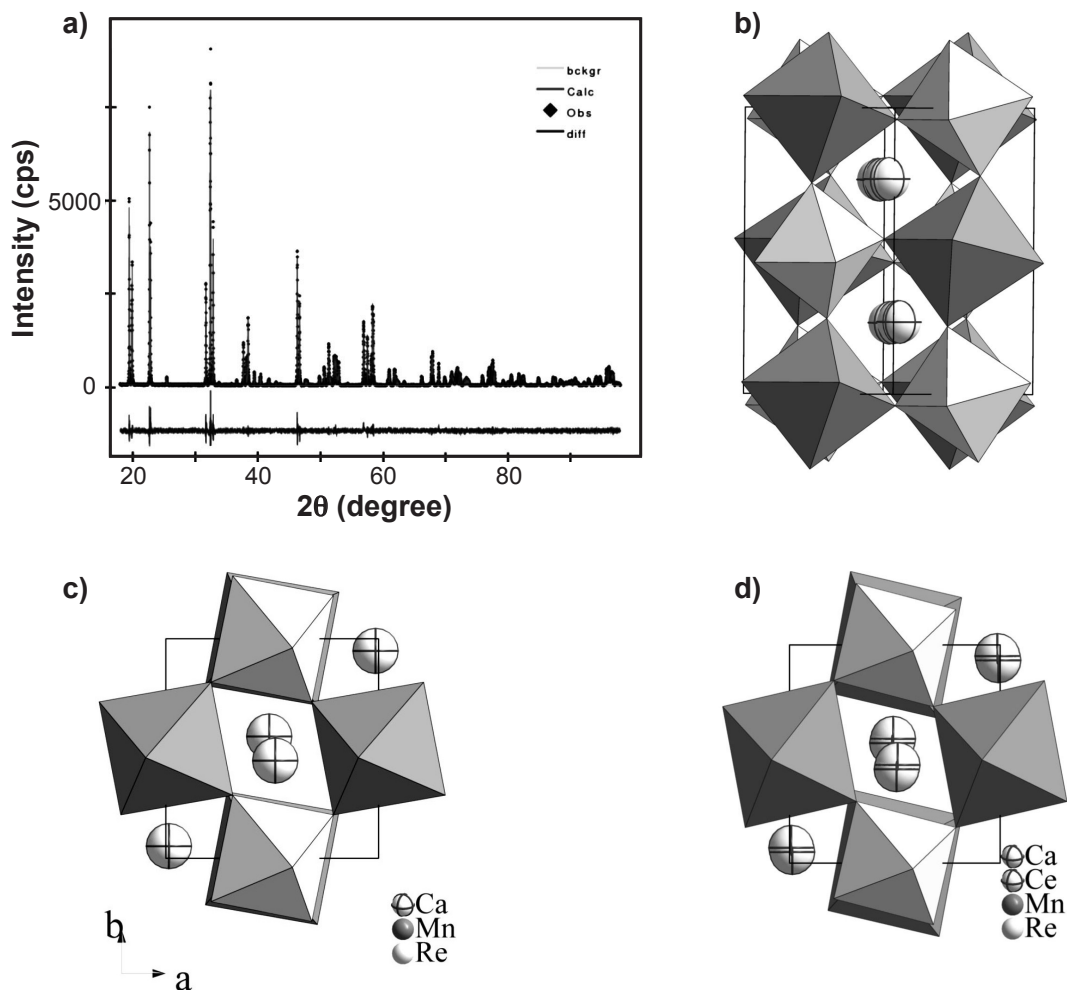


Figure 2: Schematic structure of (a) $\text{Ca}_2\text{MnReO}_6$ and (b) $\text{Ca}_{1.921}\text{Ce}_{0.079}\text{MnReO}_6$. View of the unit cell along the crystallographic (110) direction corresponding to a pseudocubic a or b axis. The dark grey octahedral represent MnO_6 and the light grey octahedral represent ReO_6 ; opposite rotations of the octahedral along the viewing direction can be seen. (c) $\text{Ca}_2\text{MnReO}_6$ and (d) $\text{Ca}_{1.921}\text{Ce}_{0.079}\text{MnReO}_6$. View along the crystallographic (001) direction showing in-phase rotations.

[Figura 2: Esquema da estrutura do (a) $\text{Ca}_2\text{MnReO}_6$ e (b) $\text{Ca}_{1.921}\text{Ce}_{0.079}\text{MnReO}_6$. Vista de célula unitária ao longo da direção cristalográfica (110) que corresponde a um pseudocúbico eixo a ou b . O octaedro cinza escuro representa o MnO_6 e o octaedro cinza claro representa o ReO_6 ; rotações apostas dos octaedros ao longo da direção podem ser vistas. (c) $\text{Ca}_2\text{MnReO}_6$ e (d) $\text{Ca}_{1.921}\text{Ce}_{0.079}\text{MnReO}_6$. Vista ao longo da direção cristalográfica (001) mostrando as rotações em fase.]

implies in tilts of neighboring octahedral in opposite directions (out of phase). The view in Fig. 2a and c along the pseudo-cubic a (or b) axis shows octahedral rotations with opposite sign and Figs. 2b and d show the view along the crystallographic c axis with the in-phase rotation of the octahedral.

It was observed that a , b and c parameters of $\text{Ca}_{1.921}\text{Ce}_{0.079}\text{MnReO}_6$ exhibit an increment as compared with $\text{Ca}_2\text{MnReO}_6$.

A visual inspection of the image (Fig. 3a) indicates that the particles have sizes ranging between 1 and 3 micrometers for $\text{Ca}_2\text{MnReO}_6$ sample. We can see at the image that there is no impurity in this sample confirming the result of X-ray diffraction data. In the $\text{Ca}_{1.921}\text{Ce}_{0.079}\text{MnReO}_6$ sample image (Fig. 3b) we see that the impurities are at the grain boundaries, which is in agreement with data from X-ray diffraction.

The average oxidation state of Mn and Re was determined by the chemical shift of the atomic absorption edge to high energy, with increasing formal oxidation state of atom. Fig.

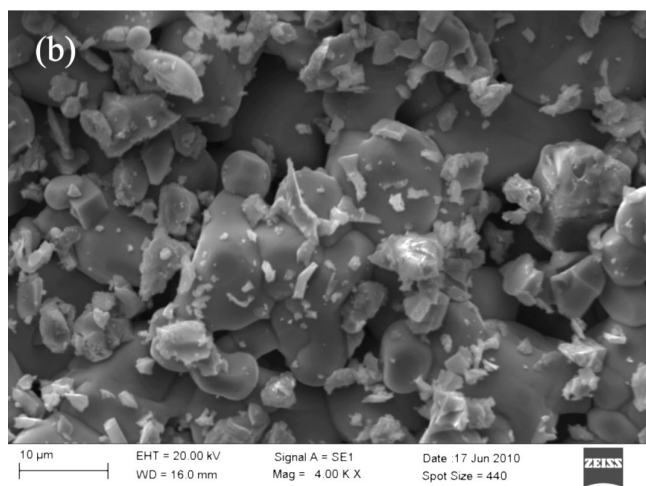
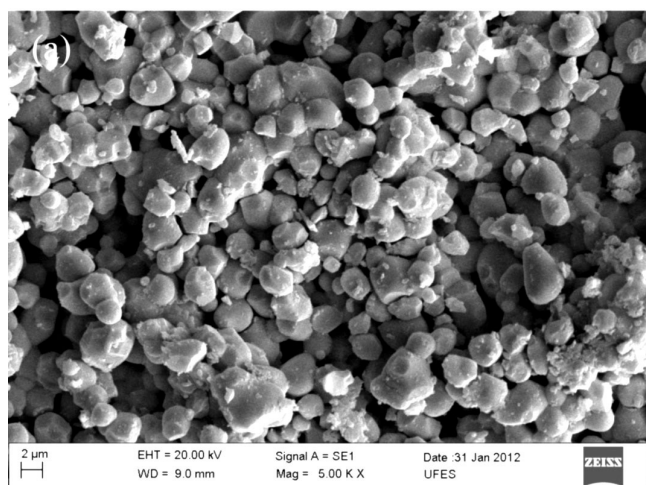


Figure 3: Secondary electron image of (a) $\text{Ca}_2\text{MnReO}_6$ and (b) $\text{Ca}_{1.921}\text{Ce}_{0.079}\text{MnReO}_6$ samples.

[Figura 3: Imagem das amostras (a) $\text{Ca}_2\text{MnReO}_6$ e (b) $\text{Ca}_{1.921}\text{Ce}_{0.079}\text{MnReO}_6$ utilizando os elétrons secundários.]

4 shows the Mn K-edge of the ordered double perovskite compounds $\text{Ca}_2\text{MnReO}_6$ and $\text{Ca}_{1.921}\text{Ce}_{0.079}\text{MnReO}_6$ including MnO (Mn^{2+}), Mn_2O_3 (Mn^{3+}) and MnO_2 (Mn^{4+}) standards. Near to normalized absorption equal 1 it is observed a closeness of the Mn edge and prominent indicated by “A” for both samples similar to MnO standard. This visual analysis shows Mn^{2+} assignments. However we concluded that the Mn shows a mixed valence in the samples. Through a linear behavior between the Mn K-edge shifts with oxidation state [24, 25] the valence of Mn was evaluated as +2.3 for the undoped sample and +2.2 for the doped sample. In addition, the prominent “B” indicates that the coordination of Mn-O octahedral in both samples is similar to MnO standard.

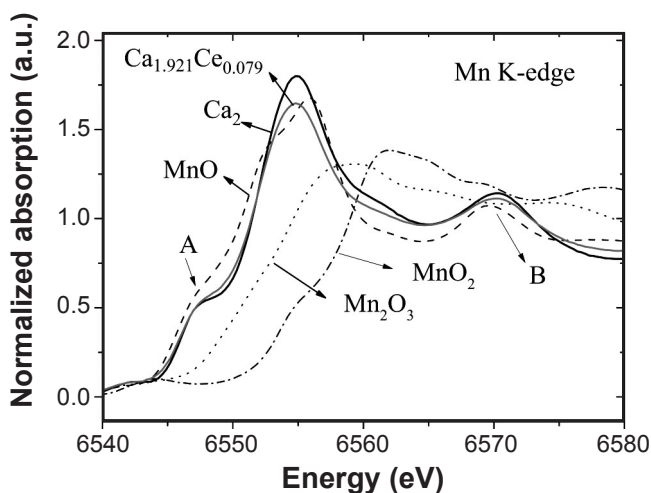


Figure 4: XANES spectra of $\text{Ca}_2\text{MnReO}_6$, $\text{Ca}_{1.921}\text{Ce}_{0.079}\text{MnReO}_6$ and MnO , Mn_2O_3 , MnO_2 standards at the MnK-edge.

[Figura 4: Borda K do Mn nos compostos $\text{Ca}_2\text{MnReO}_6$ e $\text{Ca}_{1.921}\text{Ce}_{0.079}\text{MnReO}_6$ desenhada em conjunto com os padrões de comparação MnO , Mn_2O_3 e MnO_2 .]

Fig. 5 shows the XANES spectra of the $\text{Ca}_2\text{MnReO}_6$ and $\text{Ca}_{1.921}\text{Ce}_{0.079}\text{MnReO}_6$ samples at the Re L_3 -edge including ReO_3 (+6) and ReO_2 (+4) standards. The L_3 edge for transition metals has a high intensity white line due to transitions into final d states [6], which can be correlated to the number of d holes and the oxidation state [13]. However, we used the notion of first moment (E_m) of the white-line proposed by Alp *et al.* [26] to estimate the chemical shift. This notion also was used by Popov *et al.* [6] and Corrêa *et al.* [16]. The values found were $\sim +5.7$ and $\sim +5.8$ to $\text{Ca}_2\text{MnReO}_6$ and $\text{Ca}_{1.921}\text{Ce}_{0.079}\text{MnReO}_6$ samples, respectively. These valences are in agreement with the visual analysis among white line centers of ReL_3 -edges present in ReO_3 (+6) and the samples.

We can observe in the XANES spectra (Fig. 6) that white line centers of Re L_3 -edges shift to high energy. It is associated with the increment of Re valence up to +7 as a pressure function. We can also observe a broadening of ReL_3 -edge white line with increase the pressure. The shift and shape change of the white line is related with the electronic density and Re—O, which is associated

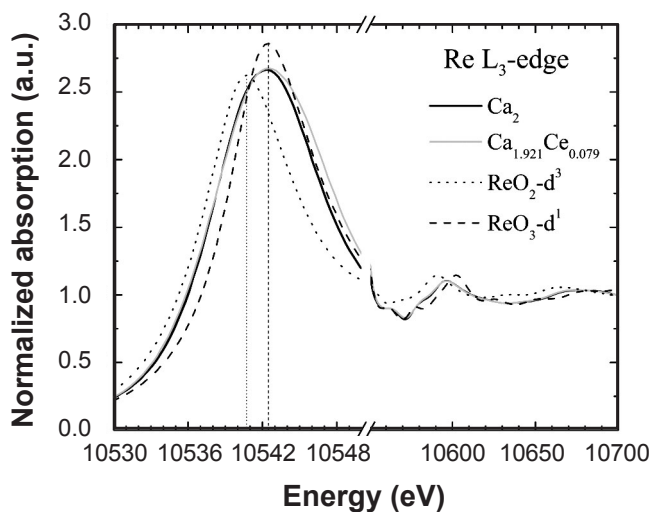


Figure 5: Re L_3 -edge of the $\text{Ca}_2\text{MnReO}_6$ and $\text{Ca}_{1.921}\text{Ce}_{0.079}\text{MnReO}_6$ compound, plotted together with the standards.

[Figura 5: Borda L_3 do rênio nos compostos $\text{Ca}_2\text{MnReO}_6$ e $\text{Ca}_{1.921}\text{Ce}_{0.079}\text{MnReO}_6$, desenhada em conjunto com os padrões de comparação.]

to octahedral distortion due to doping with Ce. However, the XANES spectra measurements of MnK-edge under different pressures showed no change in the valence of $\text{Ca}_{1.921}\text{Ce}_{0.079}\text{MnReO}_6$.

The magnetic behavior of our samples is very similar to those of $\text{Sr}_2\text{CaReO}_6$ [27] and $\text{Sr}_2\text{MgReO}_6$ [28] compounds. These compounds present geometrical frustration, which is associated to a strong competition between antiferromagnetic and ferromagnetic interactions and the absence of B and B' disorder [27-29]. One can notice in Fig. 7 a small decrease of frustration temperature in the doped sample that can be related with the increase of distortion from MnO_6 and ReO_6 octahedral.

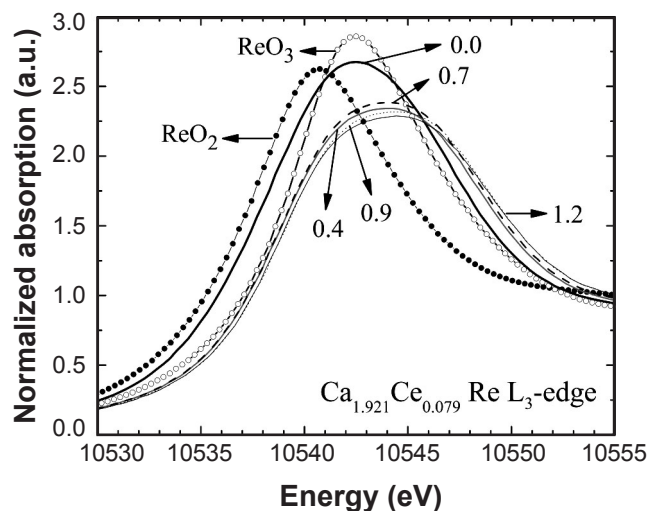


Figure 6: Re L_3 -edge of $\text{Ca}_{1.921}\text{Ce}_{0.079}\text{MnReO}_6$ compound at room pressure and under pressure up to 1.2 GPa plotted together with the ReO_2 and ReO_3 standards.

[Figura 6: Borda L_3 do rênio do composto $\text{Ca}_{1.921}\text{Ce}_{0.079}\text{MnReO}_6$ à pressão ambiente e sob pressão de até 1.2 GPa desenhada com os padrões ReO_2 e ReO_3 .]

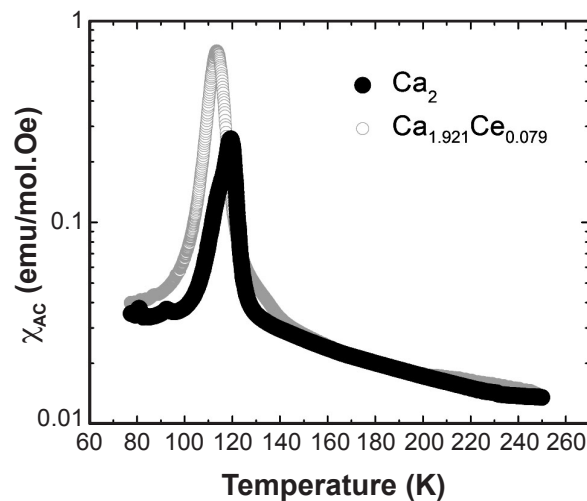


Figure 7: AC magnetic susceptibility of $\text{Ca}_2\text{MnReO}_6$ and $\text{Ca}_{1.921}\text{Ce}_{0.079}\text{MnReO}_6$ samples as function temperature with magnetic field $H_{AC} = 6$ A/m and a frequency $\nu = 448$ Hz.

[Figura 7: Susceptibilidade magnética AC das amostras $\text{Ca}_2\text{MnReO}_6$ e $\text{Ca}_{1.921}\text{Ce}_{0.079}\text{MnReO}_6$ em função da temperatura, campo magnético $H_{AC} = 6$ A/m e uma frequência $\nu = 448$ Hz.]

CONCLUSIONS

The solid solution of Ce doping in Ca-site of the $\text{Ca}_2\text{MnReO}_6$ double perovskite is limited up to ~5% by solid reaction. This solid solution was confirmed by Rietveld refinement, which indicated a monoclinic unit cell with rock-salt order of the Mn and Re ions, space group $P2_1/n$ in both samples (doped and undoped). A small amount of Ce added in Ca-site induce a small increase of lattice parameters a, b, c and Mn and Re valences. The XANES measurement of $\text{Ca}_{1.921}\text{Ce}_{0.079}\text{MnReO}_6$ showed increment of Re valence up to +7 as a pressure function. However, the Mn valences do not change with pressure. Both doped and undoped samples presented a geometric frustration, and the frustration temperature showed a small decrease in $\text{Ca}_{1.921}\text{Ce}_{0.079}\text{MnReO}_6$. The MnO_6 and ReO_6 octahedral distortion can be related with frustration temperature decreasing.

ACKNOWLEDGEMENTS

We thank LNLs for concession of beamlines (XRD1 and XAFS1) and Arcelor Mittal Co.. This work was supported by CAPES, FAPESP and CNPq, Brazil.

REFERENCES

- [1] K. -I. Kobayashi, T. Kimura, H. Sawada, K. Terakura and Y. Tokura, *Nature* **395** (1998) 677.
- [2] J. M. D. Coey, *Adv. Phys.* **48**, 2 (1999) 167.
- [3] S. A. Wolf, D. D. Awschalom, R. A. Buhrm, J. M. Daughton, S. von Molnár, M. L. Roukes, A. Y. Chtchelkanova, D. M. Treger, *Science* **294** (2001) 1488.
- [4] J. Longo, R. Ward, *J. Am. Chem. Soc.* **83**, 8 (1961) 2816.

- [5] M. W. Lufaso, P. W. Barnes, P. M. Woodward, *Acta Cryst. B* **62** (2006) 384.
- [6] G. Popov, M. Greenblatt, M. Croft, *Phys. Rev. B* **87** (2003) 024406.
- [7] D. Serrate, J. M. De Teresa, M. R. Ibarra, *J. Phys.: Cond. Matt.* **19** (2007) 023201.
- [8] J. B. Philipp, P. Majewski, L. Alff, A. Erb, R. Gross, T. Graf, M. S. Brant, J. Simon, T. Walther, W. Mader, D. Topwal, D. D. Sarma, *Phys. Rev. B* **68** (2003) 14443.
- [9] G. Popov, M. V. Lobanov, E. V. Tsiper, M. Greenblatt, E. N. Caspi, A. Borissov, V. Kiryukhin, J. W. Lynn, *J. Phys.: Cond. Matt.* **16** (2004) 135.
- [10] J. Navarro, C. Frontera, Ll. Balcells, B. Martínez, J. Fontcuberta, *Phys. Rev. B* **64** (2001) 092411.
- [11] D. Serrate, J. M. De Teresa, J. Blasco, M. R. Ibarra, L. Morellón, C. Ritter, *Appl. Phys. Lett.* **80**, 24 (2002) 4573.
- [12] D. Serrate, J. M. De Teresa, J. Blasco, M. R. Ibarra, L. Morellón, C. Ritter, *Eur. Phys. J. B* **39**, 1 (2004) 35.
- [13] J. Blasco, J. M. Michalik, J. García, G. Subías, J. M. Teresa, *Phys. Rev. B* **76** (2007) 144402.
- [14] L. Lutterotti, P. Scardi, P. Maistrelli, *J. Appl. Crystallography* **25** (1992) 459.
- [15] B. H. Toby, *J. Appl. Crystallography* **34** (2001) 210.
- [16] H. P. Corrêa, J. P. Cavalcante, D. O. Souza, E. Z. Santos, M. T. D. Orlando, H. Belich, F. J. Silva, E. F. Medeiro, J. M. Pires, J. L. Passamai, L. G. Martinez, J. L. Rossi, *Cerâmica* **56** (2010) 193.
- [17] H. C. N. Tolentino, A. Y. Ramos, M. C. M. Alves, R. A. Barrea, E. Tamura, J. C. Cezar, N. Watanabe, *J. Synchrotron Rad.* **8** (2001) 1040.
- [18] F. Ferreira, H. Correa, M. Orlando, J. Passamai Jr, C. Orlando, I. Cavalcante, F. Garcia, E. Tamura, L. Martinez, J. Rossi, F. C. L. de Melo, *J. Synchrotron Rad.* **16** (2008) 48.
- [19] L. Gomes, M. M. Vieira, S. L. Baldochi, N. B. Lima, M. Novak, N. D. Vieira Jr., S. P. Morato, A. Braga, C. Cesar, A. Penna, J. Mendes F., *J. Appl. Phys.* **63** (1988) 5044.
- [20] M. T. D. Orlando, Master's Thesis, Institute of Physics, USP, S. Paulo, SP, Brazil (1991).
- [21] R. D. Shannon, *Acta Crystallogr. Sect. A: Cryst. Phys. Diffr.Theor. Gen. Crystallogr.* **32** (1976) 751.
- [22] H. Kato, T. Okuda, Y. Okimoto, Y. Tomioka, *Phys. Rev. B* **69** (2004) 184412.
- [23] A. M. Glazer, *Acta Crystallogr. B* **28** (1972) 3384.
- [24] J. Herrero-Martín, G. Subías, J. Blasco, J. García, M. C. Sánchez, *J. Phys.: Cond. Matter* **17** (2005) 4963.
- [25] J. García, M. C. Sánchez, G. Subías, J. Blasco, *J. Phys.: Cond. Matter* **13** (2001) 3229.
- [26] E. E. Alp, G. L. Goodman, L. Soderholm, S. M. Mini, M. Ramanathan, G. K. Shenoy, A. S. Bommannavar, *J. Phys.: Cond. Matter* **1** (1989) 6463.
- [27] C. R. Wiebe, J. E. Greedan, G. M. Luke, *Phys. Rev. B* **65** (2002) 144413.
- [28] C. R. Wiebe, J. E. Greedan, P. P. Kyriakou, G. M. Luke, J. S. Gardner, A. Fukaya, I. M. Gat-Malureanu, P. L. Russo, A. T. Savici, Y. J. Uemura, *Phys. Rev. B* **68** (2003) 134410.
- [29] A. P. Ramirez, *Annu. Rev. Mater. Sci.* **24** (1994) 453. (Rec. 02/10/2012, Ac. 02/11/2012)